

pubs.acs.org/acssensors Article

# Chemiresistive Sensor Array with Nanostructured Interfaces for Detection of Human Breaths with Simulated Lung Cancer Breath VOCs

Guojun Shang, Dong Dinh, Tara Mercer, Shan Yan, Shan Wang, Behnaz Malaei, Jin Luo, Susan Lu,\* and Chuan-Jian Zhong\*



Cite This: ACS Sens. 2023, 8, 1328-1338



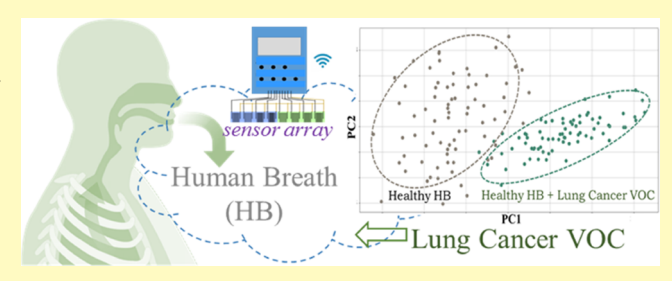
**ACCESS** I

III Metrics & More

Article Recommendations

Supporting Information

ABSTRACT: Timely screening of lung cancer represents a challenging task for early diagnosis and treatment, which calls for reliable, low-cost, and noninvasive detection tools. One type of promising tools for early-stage cancer detection is breath analyzers or sensors that detect breath volatile organic compounds (VOCs) as biomarkers in exhaled breaths. However, a major challenge is the lack of effective integration of the different sensor system components toward the desired portability, sensitivity, selectivity, and durability for many of the current breath sensors. In this report, we demonstrate herein a portable and wireless breath



sensor testing system integrated with sensor electronics, breath sampling, data processing, and sensor arrays derived from nanoparticle-structured chemiresistive sensing interfaces for detection of VOCs relevant to lung cancer biomarkers in human breaths. In addition to showing the sensor viability for the targeted application by theoretical simulations of chemiresistive sensor array responses to the simulated VOCs in human breaths, the sensor system was tested experimentally with different combinations of VOCs and human breath samples spiked with lung cancer-specific VOCs. The sensor array exhibits high sensitivity to lung cancer VOC biomarkers and mixtures, with a limit of detection as low as 6 ppb. The results from testing the sensor array system in detecting breath samples with simulated lung cancer VOC constituents have demonstrated an excellent recognition rate in discriminating healthy human breath samples and those with lung cancer VOCs. The recognition statistics were analyzed, showing the potential viability and optimization toward achieving the desired sensitivity, selectivity, and accuracy in the breath screening of lung cancer.

**KEYWORDS:** breath sensor system, volatile organic compounds, nanostructured film, chemiresistor array, sensor responses, lung cancer detection

ancer has been one of the leading causes of death by disease worldwide, accounting for nearly 10 million deaths in 2020, exceeded only by heart disease. Among all types of cancer, lung cancer is the most common cancer deaths accounting for 1.8 million deaths in 2020.2 The high mortality rate of lung cancer is mainly due to its indiscoverability in the early stages, and major symptoms such as coughing, chest pain, weight loss, etc., are often ignored by patients. The evaluation of a patient's prognosis of lung cancer requires (i) confirming the presence of the disease and (ii) staging the disease. Different methods for diagnosis and staging are used in clinical practice, including blood tests, chest X-ray, computed tomography (CT), magnetic resonance imaging (MRI), etc. A total of 85% of lung cancer cases are diagnosed at a stage when treatment is ineffective at curing the disease by utilizing current diagnostic techniques.<sup>3</sup> Overall, the 5-year survival rate is about 10-15% due to late diagnosis. However, if the disease is diagnosed at stage 1, the 5-year survival increases dramatically to 80%. With lung cancer incidences rising around the world, the need for an early detection tool is critical

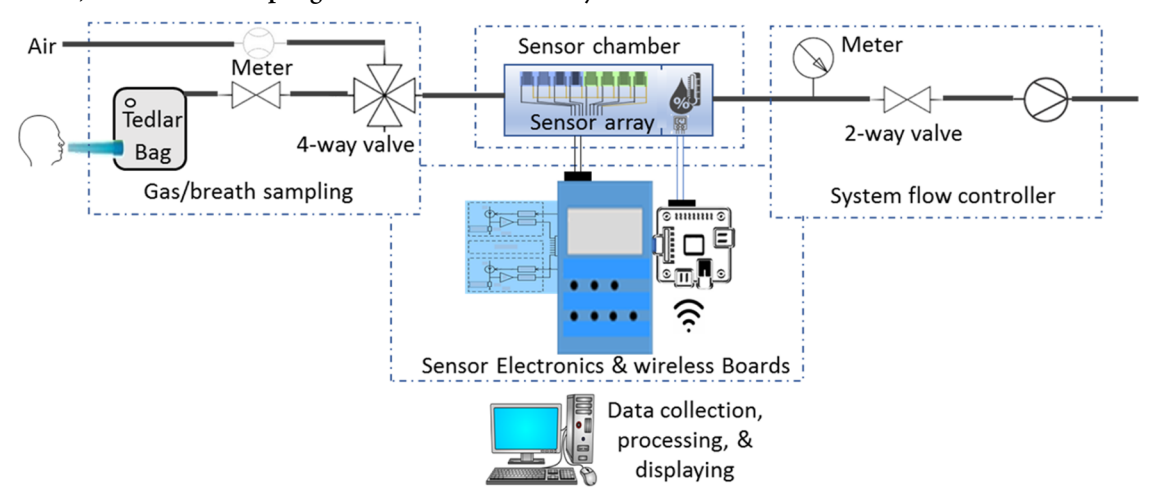
and urgent. Among many different methods, one of the emerging approaches to the early detection of lung cancer is the noninvasive detection of volatile organic compounds (VOCs) in the exhaled breath. Extensive efforts have been focused on searching for VOC biomarkers for lung cancer, either from the headspace of lung cancer cells or from the exhaled breath of patients. Since the earlier analysis of VOCs in exhaled breath from lung cancer patients using gas chromatography mass spectrometry (GC-MS),<sup>5</sup> the clinical diagnostic potential of breath analysis for lung cancer detection has risen rapidly, revealing various panels of VOCs from lung cancer breaths. One example involves a panel of 42 VOCs as

Received: December 26, 2022 Accepted: February 22, 2023 Published: March 8, 2023





Scheme 1. Block Diagram for the Integrated Breath Sensor System Consisting of a Sensor Array, Electronic Circuit and Wireless Boards, and Breath Sampling and Flow Control Subsystems



lung cancer biomarkers identified using GC-MS in combination with solid-phase microextraction.<sup>6</sup> There is increasing evidence showing that lung cancer can be detected by analyzing patients' breaths using different techniques. The detection of the VOCs is done from the identified LC VOC panel (e.g., ethyl benzene, undecane, and 2,3,4-trimethylhexane or 4-methyl-octane only for lung cancer and 2,6,6trimethyl-octane only for healthy) using a chemiresistor array consisting mostly short-length thiols featuring alkanes and hydroxyls and an aromatic motif in the ligand structures<sup>7,8</sup> (e.g., C<sub>12</sub>SH, C<sub>10</sub>SH, C<sub>4</sub>SH, 2-C<sub>2</sub>-C<sub>6</sub>SH, C<sub>6</sub>SH, tert-C<sub>12</sub>SH, 4-CH<sub>3</sub>O-PhSH, and HO-C<sub>11</sub>SH). For example, a group of VOC characteristic of lung cancer was identified from a GC column that was coupled with arrays of polymer-coated surface acoustic wave (SAW) sensors. In another study, an array of semiconductive random network of single-walled carbon nanotubes (SWCNTs) was used to detect and differentiate between the VOCs found in the breath of lung cancer patients relative to the healthy controls. 10 However, most of the widely adapted methods involve GC-MS techniques, which are highly sensitive and quantitative in the detection of VOCs, but are time consuming, expensive, and nonportable, which constitute as a major barrier for diagnostic screening and earlier detection applications. There is a clear need of portable and wireless sensors, which can be easily adapted for low-cost screening of lung cancer.

We report here a portable and wireless breath sensor array system for potential applications in screening lung cancer. The sensing interfaces in the array consist of chemiresistive thinfilm assemblies of gold nanoparticles with different nanostructures. 11,12 This sensing component is integrated into a portable manifold with an electronic component for wireless signal transduction and a flow control component for breath sampling. We demonstrate the ability of the sensor system for the discrimination of selected panels of known VOC biomarkers in human breaths from both theoretical and experimental perspectives. Theoretically, the chemiresistive responses of the sensor array to selected panels of breath VOCs with healthy and lung cancer compositions are simulated in terms of the nanostructural parameters, showing a clear indication of the ability in recognition of lung cancer VOCs. Experimentally, the sensor system is tested with healthy human breaths spiked quantitatively with the lung cancerrelevant VOCs, demonstrating the viability of discrimination between the specific VOC-spiked human breaths and controls. The results have demonstrated the potential application of our portable and wireless sensor system in a cost-effective, easy-to-use, noninvasive breath screening of lung cancer.

#### **■ EXPERIMENTAL SECTION**

Sensor Array Fabrication. Chemicals used include 11-mercaptoundecanoic acid (MUA), 1,9-nonanedithiol (NDT, 95%), 1,4-butanedithiol (BDT, 97%), 1,5-pentanedithiol (PDT, 99%), 1,6-hexanedithiol (HDT, 96%), decanethiol (DT, 96%), hydrogen tetrachloroaurate (HAuCl<sub>4</sub>, 99%), tetraoctylammonium bromide (TOABr, 99%), and sodium borohydride (NaBH<sub>4</sub>, 99%). Vapors were generated from hexane (Hx, 99.9%), benzene (Bz, 99.0%), toluene (Tl, 99.9%), 2,3,4-trimethylpentane (98%), and 2-butanone (99.0%). Water was purified with a Millipore Milli-Q water system.

Decanethiolate monolayer shell-encapsulated 2 nm diameter gold nanoparticles ( $Au_{2\,nm}$ ) were synthesized by two-phase reduction of  $AuCl_4^-$  according to Brust's standard two-phase method  $^{13}$  and a synthetic modification.  $^{14}$  The average size of the as-synthesized gold nanoparticles is  $2.0\pm0.7$  nm; details were described previously.  $^{15,16}$  Larger sizes of DT-capped gold nanoparticles were synthesized by a thermally activated processing route developed in our laboratory.  $^{15,16}$  Briefly, a measured amount of the as-synthesized DT-Au $_{2\,nm}$  solution was heated at 150 °C for 1 h, followed by several cleaning cycles via suspension in ethanol and acetone, and separated by centrifuge. Au $_{5\,nm}$  particles used in this work were prepared by this method with an average diameter of 5.2  $\pm$  0.5 nm. Morphology and size distribution details of these nanoparticles can be found in our previous reports.  $^{15,16}$ 

The nanoparticle thin films prepared for the present work included five types: (1) NDT-linked nanoparticles (NDT-Au<sub>nm</sub>), (2) BDT-linked nanoparticles (BDT-Au<sub>nm</sub>), (3) PDT-linked nanoparticles (PDT-Au<sub>nm</sub>), (4) HDT-linked nanoparticles (HDT-Au<sub>nm</sub>), and (5) MUA-linked nanoparticles (MUA-Au<sub>nm</sub>). The thin films were prepared via an "exchanging—cross-linking—precipitation" route.  $^{11,17-19}$  The reaction involved an exchange of linker molecules (NDT, BDT, PDT, HDT, MUA) with the gold-bound alkanethiolates, followed by cross-linking and precipitation via either Au S bonding at both ends of NDT, BDT, PDT, or HDT or hydrogen bonding at the carboxylic acid terminals of MUA. The reaction was carried out at room temperature with a controlled ratio of linker molecules to gold nanoparticles. Typically, the Au nanoparticle to ADT ratio was about 1:50–500 for Au<sub>2 nm</sub> and about 1:400–4000 for larger size nanoparticles. For the MUA-Au film, a 50–500 ratio of MUA to gold nanoparticles was usually used.  $^{20}$ 

The sensor arrays contain nanostructured sensing films assembled on chemiresistor devices with patterned interdigitated microelectrodes (IMEs). A typical IME pattern consists of 100 pairs of gold electrodes of 200  $\mu$ m length, 10  $\mu$ m width, 100 nm thickness, and 5  $\mu$ m spacing on a 1 mm thick glass substrate. The IMEs were fabricated by a standard microfabrication technique using the Cornell NanoScale Science & Technology Facility; details were reported previously. The thickness of the coating was below or close to the finger thickness.

Electronic Boards, Integration, and Measurement. The multichannel electronic circuit board with a wide measuring range from 30  $\Omega$  to 300 M $\Omega$  was used to measure the resistance of the chemiresistors. Through serial connections, a Raspberry Pi board was connected to the electronic circuit board and was used for wireless data transmission. All experiments were performed at the same conditions as the standard measurement. Compressed air gas (breathing grade, Airgas) was used as a carrier gas. The gas flow was controlled by a calibrated mechanical flow meter (Matheson U002). The IME devices were housed in a Teflon chamber with tubing connections to vapor and air sources; the electrode leads were connected to the electronic circuit board. Human breath samples were injected into the system for testing. The sensing experiments were carried out by monitoring the chemiresistors and environmental sensors (relative humidity and temperature sensors) while exposing to human breath samples. Before exposing to human breath samples, the test chamber was purged with compressed air for 1 h to establish the baseline. A typical exposing cycle included a 1 min vacuum step, followed by a 3 min exposure to samples and ended with a 2 min air cleaning step.

All experiments were performed at room temperature,  $22\pm1~^\circ\text{C}.$   $N_2$  gas (99.99%, Airgas) was used as a reference gas and as a diluent to change the vapor concentration by controlling the mixing ratio. The gas flow was controlled by a calibrated Aalborg mass-flow controller (AFC-2600). Different concentrations of vapors were generated using an impinger system. The vapor concentration (ppm moles per liter) was calculated from the partial vapor pressure and the mixing ratio of vapor and  $N_2$  flows.

Breath samples were collected with healthy subjects including three males and three females. All subjects were asked to take 3–5 deep breaths before sample collections. Alveolar breath samples were collected into 1 L Tedlar sampling bags through 1 feet long silicone tubing by directly blowing via plastic mouthpiece as shown in Scheme 1. The volunteers were asked to be fasting for at least 12 h prior to their alveolar breath collection. All samples were analyzed 5 h after collection, and five repeated tests were conducted.

Simulated lung cancer patients' breath samples were prepared by spiking lung cancer-related volatile organic compounds (VOCs) to the as-collected human subjects' breath samples. The lung cancer VOCs chosen are toluene, 2-butanone, and 2,3,4-trimethyl-pentane, which were generated by the gas flow and mixing method. The gas flow was controlled by an array of calibrated Aalborg mass-flow controllers (AFC-2600), details of which were previously described. 16,17

Simulation and Data Analysis Methods. Random forest (RF) is a classification method, but it can also provide feature importance. A forest contains many decision trees, each of which is constructed with randomly sampled features. Output was computed by a majority vote of all decision trees. First, the overall node probability could be calculated as the number of samples that reach the node divided by the total number of samples. Next, feature importance was calculated by the product of decrease in node impurity (measured by the Gini index) and the overall node probability. The "Random Forest Classifier" algorithm in the Scikit-learn Python library was used to obtain feature importance. The inputs for random forest algorithm are noise-added sensor array responses from eight individual sensors. Last, the output of feature importance was used as criteria for feature selection of sensor arrays. Higher values of feature importance imply more important features. Feature selection data were standardized before applying the principal component analysis (PCA) algorithm.

#### RESULTS AND DISCUSSION

In this section, we first describe the results from theoretical simulations of nanostructured sensor arrays' responses to the adsorption of different panels of VOCs and different concentrations in connection with simulated breaths. This description is followed by the discussion of the results from experimental sensor responses to selected panels of VOCs of different concentrations and human breaths spiked with selected VOCs as simulated lung cancer breaths.

Simulation of Sensor Array Responses to Selected Panels of Breath VOCs. Theoretical Model and Simulation Results. Since the first report of the monolayer thiolencapsulated gold nanoparticles as chemiresistor thin films, numerous researchers have explored the chemiresistive properties and applications of such nanoparticle assemblies. The underlying mechanism involves a thermally activated conduction path<sup>22</sup>

$$\frac{\Delta R}{R_{\rm i}} = e^{\beta \Delta \delta} e^{\Delta E_{\rm a}/k_{\rm b}T} - 1 \tag{1}$$

where  $\Delta R/R_i$  is the sensor response known as the relative resistance change,  $\beta$  is the tunneling decay constant,  $\delta$  is the edge-to-edge interparticle distance,  $E_a$  is the activation energy,  $k_b$  is the Boltzmann constant, and T is the temperature, where the activation energy  $(E_a)$  is

$$E_{\rm a} = \frac{e^2}{8\pi\varepsilon_0\varepsilon_r} \left( \frac{1}{r} - \frac{1}{r+\delta} \right) \tag{2}$$

where  $e=1.6\times 10^{-19}$  C,  $\varepsilon_0$  is the dielectric constant and  $\varepsilon_r$ , r, and  $\delta$  represent the dielectric constant of the particle medium, particle radius, and interparticle distance, respectively. Considering the change of the dielectric constant in the thin-film medium upon vapor adsorption, the  $\Delta E_a$  can be then expressed as

$$\Delta E_{\rm a} = \frac{e^2}{8\pi\varepsilon_0} \left[ \frac{1}{\varepsilon_{\rm sw}} \left( \frac{1}{r} - \frac{1}{r+\delta+\Delta\delta} \right) - \frac{1}{\varepsilon_{\rm film}} \left( \frac{1}{r} - \frac{1}{r+\delta} \right) \right] \tag{3}$$

where  $\varepsilon_{\rm sw}$  represents the dielectric of the analyte swollen ligand matrix,  $\varepsilon_{\rm film}$  is the dielectric of the sensing film, and  $\Delta\delta$  is the change of the interparticle distance upon sorption of the solvent. By substituting eq 3 into eq 1, the sensor response  $\Delta R/R_{\rm i}$  equation can be expressed as

$$\begin{split} \frac{\Delta R}{R_{\rm i}} &= \exp(\beta \Delta \delta) \\ &\times \exp\left\{\frac{e^2}{8\pi \epsilon_0 k_{\rm b} T} \left[\frac{1}{\epsilon_{\rm sw}} \left(\frac{1}{r} - \frac{1}{r+\delta + \Delta \delta}\right) \right. \right. \\ &\left. - \frac{1}{\epsilon_{\rm film}} \left(\frac{1}{r} - \frac{1}{r+\delta}\right) \right]\right\} - 1 \end{split} \tag{4}$$

where, in addition to the regular constants ( $e=1.6\times10^{-19}$  C,  $\varepsilon_0=8.854\times10^{-12}$  F m<sup>-1</sup>,  $R=1.38\times10^{-23}$  J K<sup>-1</sup>), T is temperature,  $\varepsilon$  is the dielectric constant of the medium,  $\beta$  is the electron coupling term, and r and d (= $\delta$ ) represent the particle radius and interparticle spacing (nm), respectively.<sup>23,24</sup> The dielectric of the analyte swollen thin-film matrix  $\varepsilon_{\rm sw}$  can be estimated as the volume-weighted average of the dielectric of the analyte and the sensing film<sup>25</sup>

$$\varepsilon_{\rm sw} = f_{\rm ana} \, \varepsilon_{\rm ana} + (1 - f_{\rm ana}) \varepsilon_{\rm film} \tag{5}$$

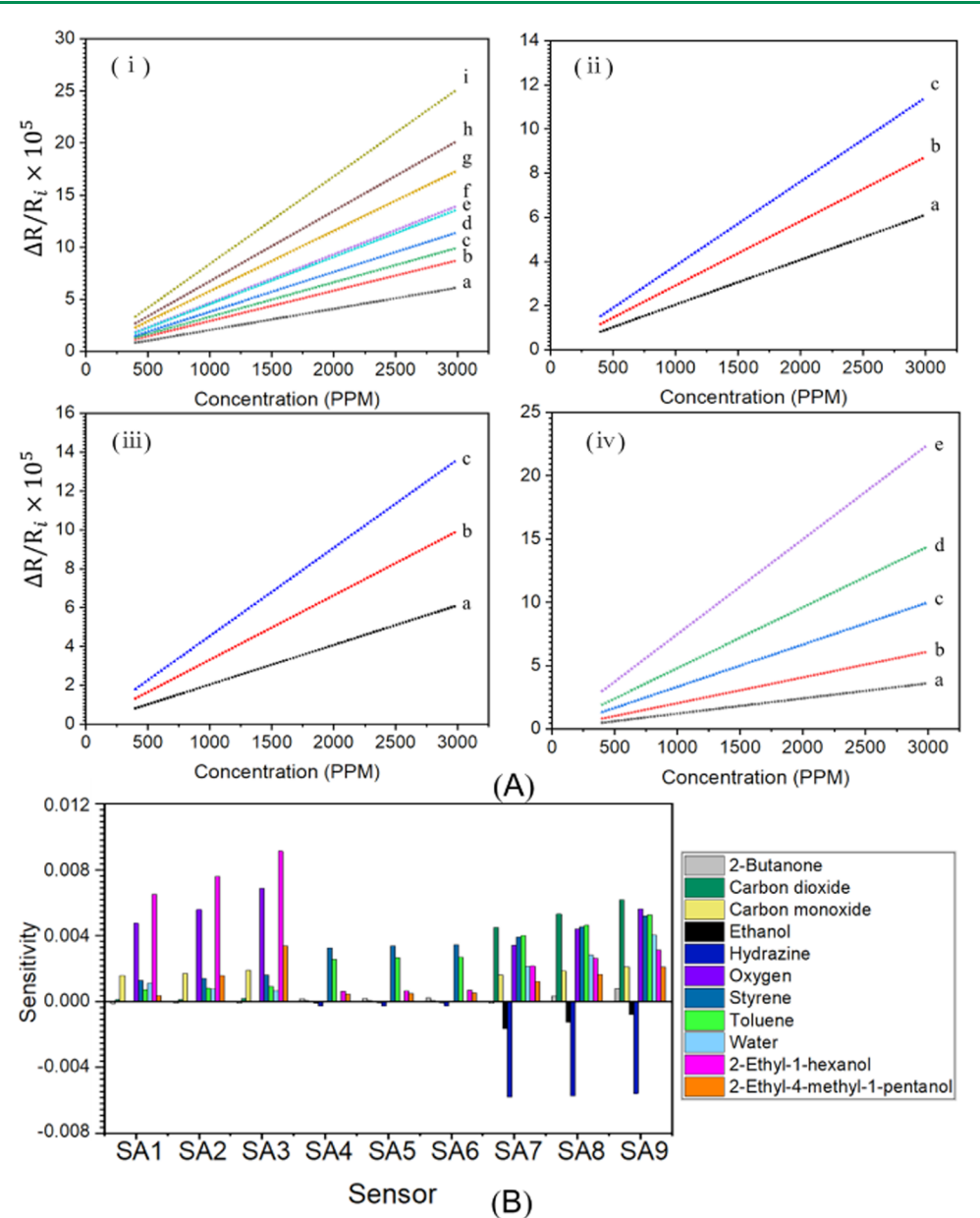


Figure 1. (A) Plots of response  $(\Delta R/R_i)$  of a sensor array (PE type) of different parameters in response to VOCs. (i) Ethanol of different concentrations on a sensor array with different particle radii (r, nm) and interparticle distances  $(\delta, \text{nm})$ ,  $(r, \delta)$ : a, (1.0, 0.844); b, (1.0, 1.75); c, (1.0, 2.78); d, (2.5, 0.844); e, (2.5, 1.75); f,  $(2.5, \delta = 2.78)$ ; g, (5.0, 0.844); h, (5.0, 1.75); and i, (5.0, 2.78). (ii) Ethanol vapor on a sensor array  $(r = 1.0 \text{ nm}; \delta = 0.844 \text{ (a)}, 1.75 \text{ (b)}$ , and 2.78 nm (c)). (iii) Ethanol vapor on a sensor array  $(\delta = 0.844 \text{ nm}; r = 1.0 \text{ (a)}, 2.5 \text{ (b)}$ , and 5.0 (c) nm). (iv) Alcohol vapors (a: methanol, b: ethanol, c: 1-propanol, d: 1-butanol, and e: 1-pentanol) on a sensor array  $(r = 1.0 \text{ nm}, \delta = 0.844 \text{ nm})$ . (B) Comparison of the simulated response sensitivities for the indicated panel of VOCs with 40-400 ppb (V) on a nine-sensor array derived from nanoparticle assemblies with PE-type (SA1-SA3), PEO-type (SA4-SA6), and P4HS-type (SA7-SA9) structure characteristics (note that VOCs with 1-40 and 400-7 ppm (V) ranges were also simulated, showing similar trend but subtle differences in sensitivities).

where  $\varepsilon_{\rm ana}$  is the dielectric of the analyte and  $f_{\rm ana}$  represents the volume fraction of the analyte within the organic matrix, which can be expressed as

$$f_{\rm ana} = \frac{V_{\rm ana}}{V_{\rm film} + V_{\rm ana}} = \frac{KC_{\rm v}MM_{3}^{4}\pi r_{\rm eff}^{3}}{\rho_{\rm ana}V_{\rm film} + KC_{\rm v}MM_{3}^{4}\pi r^{3}}$$
(6)

where  $V_{\rm ana}$  is the volume of the sorbed analyte within the sensing film,  $V_{\rm film}$  is the volume of the sensing film, K is the partition coefficient,  $C_{\rm v}$  is the concentration of the analyte, MM is the molar mass of the analyte,  $\rho_{\rm ana}$  is the density of the analyte, and  $r_{\rm eff}$  is the effective radius of the particle, which

includes the gold nanoparticle core and the ligand shell with a thickness of  $\delta/2$ . Thus, the  $V_{\rm film}$  can be expressed as

$$V_{\rm film} = \frac{4}{3}\pi (r_{\rm eff}^{3} - r^{3}) \tag{7}$$

The interparticle distance change  $\Delta\delta$  reflects the relative volume increase of the ligand matrix upon analyte adsorption, which can be expressed as

$$\Delta \delta = 2r_{\text{eff}} \left( \sqrt[3]{\frac{\rho_{\text{analyte}} V_{\text{film}}}{\rho_{\text{analyte}} V_{\text{film}} - \frac{4}{3} \pi K C_{\text{v}} \text{MM} (r_{\text{eff}}^{3} - r^{3})}} - 1 \right)$$
(8)

where the partition coefficient (K) is related to the permeability and correlated with the Hansen solubility component, which can be expressed as  $^{27}$ 

$$K = \frac{A}{D} \exp \left\{ \sum_{i=1}^{3} C_{i} [CED_{i(analyte)} - CED_{i(film)}] \frac{MV_{analyte}}{RT} - C_{4} \frac{MV_{analyte}}{RT} \right\}$$
(9)

where A is the pre-exponential factor related to entropy, D is the diffusion coefficient of the analyte in air,  $C_i$  is the best fit coefficient,  $C_4$  is the best fit coefficient to the molar volume,  $CED_{i(analyte)}$  is the ith component of cohesive energy density for a given analyte,  $CED_{i(film)}$  is the ith component of cohesive energy density for the sensing film, and  $MV_{analyte}$  is the molar volume of a given analyte.

As described, the electrical conductivity of the nanocomposite film follows the thermally activated conduction pathway in which the activation energy increases with the interparticle distance and decreases with the particle size. 23,24 Equation 4 expresses the change of the electrical conductivity in response to VOC adsorption in the film in terms of thermally activated conduction theory as the relative change in resistance  $(\Delta R/R_i)^{23-25}$  There are two important parameters,  $\Delta\delta$  and  $arepsilon_{
m sw}$ , which are the change in interparticle distance  $(\Delta\delta)$ and the dielectric constant of the medium  $(\varepsilon_{\mathrm{sw}})$  upon the adsorption of VOCs in the sensing film, respectively. Both  $\Delta\delta$ and  $\varepsilon_{\rm sw}$  depend on the particle size, the interparticle distance, and most importantly the vapor concentrations  $(C_v)$ .  $\varepsilon_{sw}$ contains contributions of the dielectric permittivity properties of the VOC and the VOC-adsorbed film. A common characteristic of  $\Delta\delta$  and  $arepsilon_{\mathrm{sw}}$  is their dependencies on the vapor partition equilibrium constant (K) of the VOC in the film and  $C_v$  in the gas phase. One approach to the theoretical simulation involves the use of solubility parameters of the VOC and the thin film to assess the K, which is a numerical estimate of the degree of interaction between VOCs and films  $(\partial_{\text{total}}^2 = \partial_{\text{d}}^2 + \partial_{\text{p}}^2 + \partial_{\text{h}}^2$ , where  $\partial_{\text{d}}^2 =$  dispersion component,  $\partial_{\text{p}}^2$ = polar component, and  $\partial_h^2$  = hydrogen bonding component). Our simulations adopted the Hansen solubility parameters,<sup>2</sup> and the cohesive energy densities for the polymers derived molecular dynamics calculation and fitting coefficients.<sup>26,27</sup> Based on our design of the nanocomposite sensing films for the targeted VOCs and breaths, we considered a similarity approach to polymer-carbon sensing films, including polyethylene (PE), poly(ethylene oxide) (PEO) (including poly-(ethylene glycol) (PEG), molecular weight of PEG < PEO), and poly(4-hydroxy styrene) (P4HS) (or poly(4-vinylphenol), PVP). 26,28-30 The MD-derived interaction energy data are used for the simulation in terms of solubility parameters. <sup>26</sup> We used the parameters derived for the carbon-particle embedded PE-, PEO-, and P4HS-like structures by alkyl-dithiolate (e.g., noanedithiol NDT) linkers in combination with alkanethiol capping molecules (RS), carboxyl-functionalized alkylthiol (e.g., mercaptoundecanoic acid MUA) linkers in combination with RS, and composite matrix-derived dendrons/cellulose/ graphene in combination with MUA linkers, respectively.

Since solubility parameters are not available for the thiol molecules, we performed the theoretical simulations for the thin-film assemblies of thiolate-stabilized gold nanoparticles as chemiresistor sensors in response to different VOCs and breaths using polymeric structures, which have available solubility parameters.<sup>26</sup> The selected polymer types feature functional groups or backbones similar to the thiol molecules in the thin-film assemblies of nanoparticles. To assume reasonable solubility parameters for the thin films, the solubility parameters for three polymer matrices<sup>26</sup> were adapted in the simulation, including the polyethylene (PE) matrix for the NDT-Au<sub>nm</sub> film, poly(ethylene oxide) (PEO) matrix for the MUA-Au<sub>nm</sub> film, and poly(4-hydroxy styrene) (P4HS) matrix for the dendron-Au<sub>nm</sub> film. For each sensor array, three different nanoparticle sizes and three different interparticle distances were selected for simulations. The structural and physical parameters for the three types of arrays used in this work are summarized in Table S1. Ten common VOCs were selected as testing vapors, including methanol, ethanol, 1-propanol, 1-butanol, 1-pentanol, acetone, benzene, styrene, toluene, and *n*-hexane, in the concentration range of 400-3000 ppm.

Figure 1Å shows a representative set of data for an array constructed in terms of the interparticle molecular structure type, gold nanoparticle radius, and interparticle distance to illustrate the simulated sensor response sensitivity to ethanol vapor of different concentrations.  $\Delta R$  is the resistance changes in response to vapor exposure, and  $R_i$  is the initial resistance of the sensing film. The sensitivity is reflected by the relative differential resistance change,  $\Delta R/R_i$ , vs the vapor concentration, C (ppm). The PE sensor array exhibit linear response toward ethanol concentrations. Similar linear relationships were found for the other VOCs with subtle differences in sensitivities (i.e., slopes).

The sensor array features a combination of the PE-, PEO-, and P4HS-like structures in the presence of the assembled NPs with variations in interparticle distances by the linker molecules, which can be achieved based on our previous and recent works using gold NPs of three different sizes (e.g., 2, 5, and 10 nm) linked by bifunctional molecules (e.g., NDT, MUA, MHA, MBA, etc.) and dendrons as linkers and cellulose, carbon nanotubes, and graphene as the sensing composite scaffolds. These sensors display different sensitivities and negative- or positive-going responses depending on the VOC—film combinations (Figure 1B), which are also consistent with our experimental results.

The sensitivities of the PE sensor array (slopes) are compared with those of the NDT-Au<sub>nm</sub> sensors. 11 The response sensitivities for the simulated PE sensor array are slightly lower than those of NDT-Aunm sensors, exhibiting a similar magnitude (10<sup>-5</sup> ppm<sup>-1</sup>). The similarity demonstrates that the simulation based on the PE-type sensor array is a viable approach to study the sensor response characteristics of the NDT-Au<sub>nm</sub> sensors. As the gold nanoparticle size and interparticle distance changed, the response sensitivities for the PE sensor arrays to ethanol changed. Figure 1A(ii,iii) shows a representative set of data to illustrate the simulated sensor response characteristics to alcohol vapors with different nanoparticle sizes and interparticle distances. As shown in Figure 1A(ii) for ethanol vapor on an array with 2 nm gold nanoparticle size and three different interparticle distances (0.844, 1.75, and 2.78 nm), the response sensitivity increases with the interparticle distance. This finding is consistent with the NDT-Au<sub>nm</sub> sensor behavior both qualitatively and quantitatively. From the qualitative aspect, as the interparticle distance increases, the interaction space between the sensing

film backbone and vapor molecules increases, leading to the sensor response sensitivity increase. Quantitatively, such a sensitivity increase is also in line with the sensor response simulation eq 4. At a given particle radius, the increase of the interparticle distance increases the relative differential resistance change,  $\Delta R/R_i$ , and thus the response sensitivity. At a given interparticle distance (e.g., 0.844 nm), the change of the nanoparticle radius leads to a change of the sensor response sensitivity, as shown in Figure 1A(iii) by a representative set of simulated PE sensor response sensitivity in response to ethanol vapor for different gold nanoparticle radii (1, 2.5, and 5 nm). Similar results were also observed with other VOCs. Simulations of the sensor response of the PE-type sensor array to alcohol vapors of different carbon number were also performed, as shown in Figure 1A(iv) for PE-Au<sub>2 nm</sub>- $\delta$  0.844 nm in response to five alcohols with increasing carbon numbers. The sensitivity clearly increases with the alcohol's carbon number, showing a sensitivity of  $1.488 \times 10^{-6} \text{ ppm}^{-1}$ for methanol and  $2.440 \times 10^{-4} \text{ ppm}^{-1}$  for 1-pentanol. This indicates a stronger hydrophobic interaction between the sensing film backbone and alcohol molecules with a longer carbon chain.

Principal Component Analysis of the Simulated Sensor Responses. PCA is used for variable dimension reduction (feature extraction) and clustering purpose. The simulated responses of the three different types of sensor arrays to different lung cancer-related VOCs were analyzed. We first compared some of the simulated results with the experimental data. Figure 2A shows the PCA result for an example group

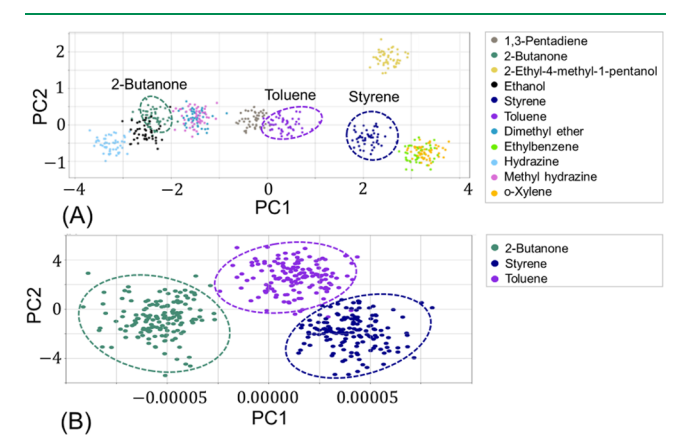


Figure 2. PCA plot for simulated and experimental response data. (A) For the indicated group of VOCs with 40–400 ppb (V) on a 9-sensor array derived from nanoparticle assemblies with PE-, PEO-, and P4HS-type structure characteristics (note that VOCs with 1–40 and 400–7 ppm (V), ranges were also simulated, showing a similar trend but subtle differences in sensitivities and effective separation). (B) A set of experimental sensor data from a sensor array in response to three of the VOCs, 2-butanone, toluene, and styrene.

VOCs based on the simulation data of the nine-sensor array. Clearly, the major VOCs can effectively be separated as shown by PCA results. The separations among different VOCs demonstrate the viability of the sensor array in achieving high-recognition sensitivity and selectivity, indicating a promising pathway for the development and optimization of the sensor array combinations for the detection of the identified breath VOC biomarkers. Figure 2B shows the PCA result for an experimental data set for three VOCs (toluene, styrene, and 2-

butanone) using a sensor array. There is a clear agreement between the simulation and the experiment results.

The sensor responses to lung cancer-related VOCs have also been examined using simulated VOCs. VOCs were selected from a panel of lung cancer-related VOCs (Table S26) for sensor response simulations. Based on the abundance of the VOCs in human breaths, the selected VOCs fall into three categories: (i) the abundance is greater in the breath from healthy people (HP) than those in lung cancer (LC) patients (HP > LC) (e.g., hydrazine, 2-butanone, 2,2,3-trimethylhexane, etc.), (ii) the abundance is greater in LC breath than those of HP (LC > HP) (e.g., toluene, styrene, o-xylene, dimethyl ether, 1,3-pentadiene, methyl hydrazine, ethanol, ethyl benzene, 2-methly-hexane, etc.), and (iii) the LC breathspecific VOCs (LC only) (e.g., 2-ethyl-1-hexanol, 2-ethyl-4methyl-1-pentanol, 2,3,4-trimethyl-pentane, 4-methyl-octane, etc.). The PCA results for the simulated sensor responses to the lung cancer-related VOCs are shown in Figure 2A. It is evident that the lung cancer-specific VOC, 2-ethyl-4-methyl-1pentanol, is well separated from other VOCs. The two vapors from the HP > LC group, 2-butanone, and hydrazine, fall into a cluster group located at the left bottom area of the PCA plot and partially overlapped with some of the vapors from the LC > HP group. It can be concluded based on the PCA results that the three types of sensor arrays are able to distinguish between the VOCs from healthy people and the VOCs from lung cancer patients' breaths, thus showing a great potential for application in lung cancer breath sensors.

This feasibility is further studied in the concentrations of the lung cancer-specific VOCs. A set of simulated lung cancer breaths with the LC-specific VOCs in different concentration ranges is used to mimic the different stages of lung cancer. Two LC-specific VOCs were selected from the panel of the 42 lung cancer-related VOCs and were mixed with 15% oxygen, 5% water vapor, 4% CO<sub>2</sub>, and ppm-level CO to mimic the human breath composition.

PCA analysis is performed on the normalized sensor responses from the simulation, as shown in Figure 3. It is evident that, as the concentration of LC-specific VOCs increases (Figure 3A–C), there is an indication of better separation between the LC-specific VOCs and the normal VOCs

By comparing the PCA results of the sensor responses to the simulated LC breaths in different concentration ranges with and without the LC-specific VOCs, distinct clusters are observed in the PCA plots (Figure 4). It is evident that the separation distance for three LC-specific VOC groups in different concentration ranges from that without the LCspecific VOCs increases with the VOC concentration, demonstrating the quantitative aspect of the sensor array in recognition of breaths with LC-specific VOCs in different concentrations. PCA analysis of the simulation data (Figure 1B) for different concentrations of VOCs has demonstrated the possibility to separate H breath from LC breath with different stages (Figure 4). First, the separation depends on the VOC concentrations (Figure 1B), supporting the feasibility of the separation of LCs with different stages. Second, the separation of the LC breaths of the three different concentration ranges and the H breath is also shown to be highly viable (Figure 4). We also compared the results of PCA separation between H and LC breaths in terms of the number of array elements (9 vs 3), showing improvement of the

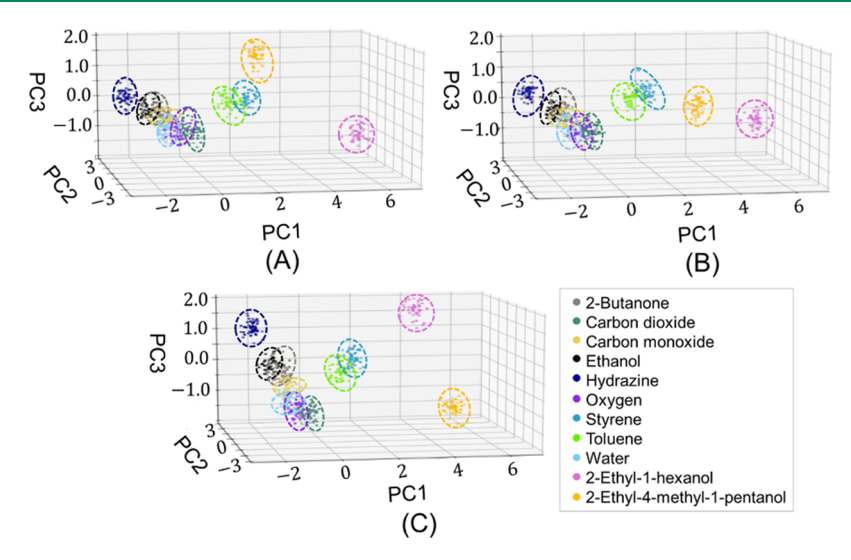
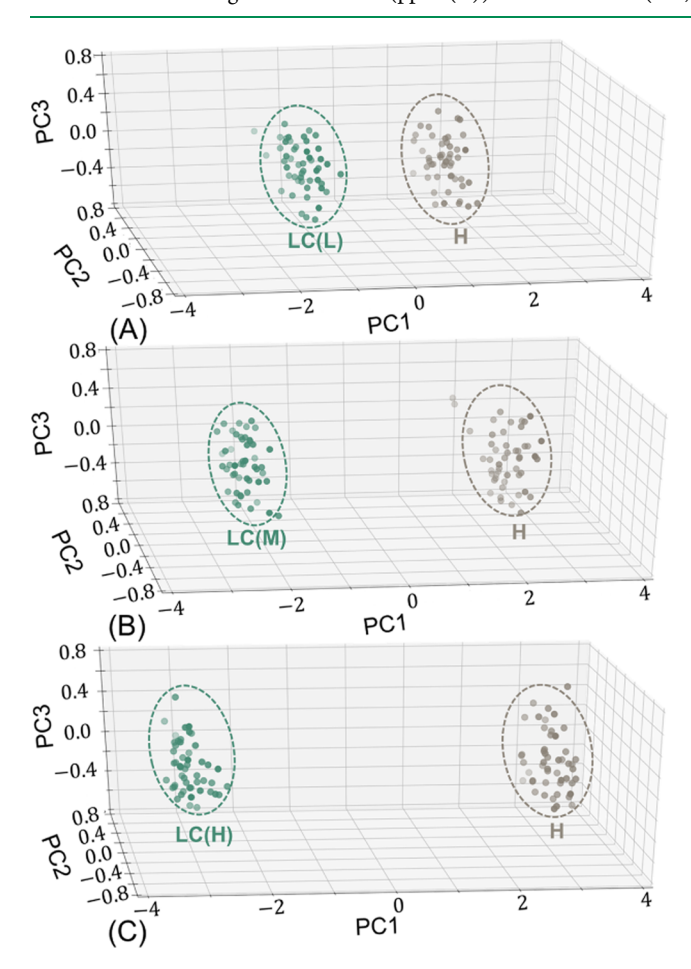


Figure 3. PCA plots for simulated sensor responses to breaths with LC-specific VOCs. (A–C) The VOCs in (A) low, (B) middle, and (C) high concentrations in lung cancer breaths (ppm (V)): 0.0001–0.001 (low, A), 0.002–0.02 (middle, B), and 0.03–0.3 (high, C).



**Figure 4.** 3D PCA plots for simulated sensor responses to the breath VOC panel with and without the LC-specific VOCs with three different concentration ranges (ppm (V)): (A) 0.0001–0.001 (low), (B) 0.002–0.02 (middle), and (C) 0.03–0.3 (high).

separation with increasing the number of array elements and ample room for improvement for mixtures of VOCs.

Experimental Sensor Array Responses to Human Breath Samples with Lung Cancer-Specific VOCs. Sensor Response Characteristics. The experimental response charac-

teristics were determined for the sensor array system with different nanostructured sensing materials in response to human breath samples with and without lung cancer-specific VOCs. The collection of the human breath samples is detailed in the Experimental Section. Figure 5A shows a representative example of the sensor response profile; we first show the results from the experimental determination of the limit of detection (LOD) for the sensor array system. We analyzed the sensor response to different VOCs in the low concentration range. Figure 5A,B shows a representative set of data for hexane at the ppm-level concentration. The response exhibits a linear relationship vs. hexane concentration (Figure 5B), with the response sensitivity being  $2.67 \times 10^{-4}$ . The LOD was estimated from the sensitivity and the three times of standard deviation ( $\sigma$ ) of the background noise ( $\sigma$  of  $\Delta R/R_i \sim 4.65 \times$ 10<sup>-7</sup>). The estimated LOD is 6 ppb for hexane. Similar LODs were obtained for other VOCs, ranging from sub ppb to a few ppb.

The response profiles for an eight-sensor array consisting of sensing films, i.e., MUA-Au<sub>2 nm</sub>, MUA-Au<sub>5 nm</sub>, BDT-Au<sub>2 nm</sub>, BDT-Au<sub>5 nm</sub>, PDT-Au<sub>2 nm</sub>, HDT-Au<sub>2 nm</sub>, NDT-Au<sub>2 nm</sub>, and NDT-Au $_{5\,\mathrm{nm}}$ , in response to human breath samples and those spiked with lung cancer-specific VOCs were collected. The tested lung cancer-specific VOCs are based on commercially available ones, including toluene, 2-butanone, and 2,3,4trimethyl-pentane, each with a concentration of 9 ppm. Figure 5C shows a typical set of the sensor array response data for healthy human breaths. Despite the highly humidified human breath samples, almost no differences were observed in multiple replicas of the testing in terms of the response profiles. The data were highly reproducible, and the sensor array was stable under the testing condition. Figure 5D shows a typical set of the sensor array response data for healthy human breaths spiked with three lung cancer-related VOCs. Again, the responses are highly reproducible for each replica. In comparison with the data in Figure 5C, the sensor array showed a slightly higher sensor response magnitudes for the breaths spiked with the lung cancer-related VOCs, which will be analyzed by PCA to demonstrate the viability of the sensor array to distinguish between the healthy and lung cancer breaths.

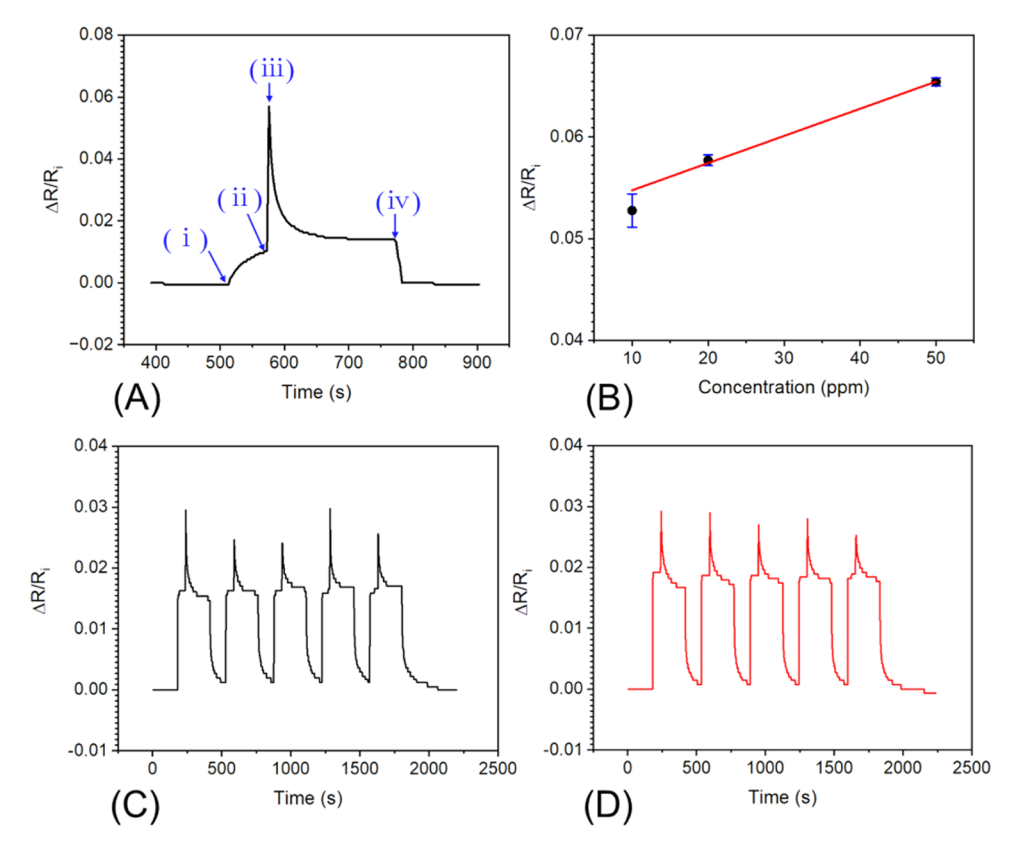


Figure 5. (A) Typical sensor response profile: (i) air purge (2 min), (ii) air suction by a diaphragm pump (1 min), (iii) sample introduction by a releasing valve connecting to the sample bag (3 min), and (iv) air purge (2 min). (B) Plot of the sensor response vs hexane concentration. (C–D) Two typical sets of sensor response profiles to human breath samples (C) and human breath sample spiked with lung cancer-specific VOCs ((D), toluene, 2-butanone, and 2,3,4-trimethyl-pentane, each at 9 ppm).

Principal Component Analysis of the Experimental Sensor Responses. The responses of the eight-sensor array to human breath samples with and without lung cancer-specific VOCs are analyzed by PCA. The first two principal components (PC1 and PC2) are used as the classification features. PCA analysis is performed with the sensor response data from each individual human breath samples with and without lung cancer-specific VOCs, which is shown in Figure 6A–F. It is evident that the individual breath samples with and without lung cancer-specific VOCs can be well separated. The results demonstrate that the sensor array is promising for distinguishing the human breath samples with and without lung cancer.

Figure 6G shows the PCA plots of the sensor response data to human breath samples with and without lung cancer-specific VOCs. It is evident that there are two almost-distinct cluster groups representing the healthy and lung cancer breath samples. There is a small overlap between the two groups largely due to the limited sample sizes at this point of time.

The sensitivity and selectivity of the above data are further assessed by performing data analysis using multiple neural network modules with the Random Forest (RF) algorithm for pattern recognition. The PCA results were analyzed in terms of the classification rate, sensitivity, and selectivity. The Random Forest classifier obtains 93.99% accuracy across testing data and successfully classified 86.96% of the lung cancer breath samples. For healthy breath samples, the RF model is shown to reach a 100% accuracy.

The stability of the sensor responses to human breath samples with ("LC") and without spiked lung cancer-specific

VOCs ("healthy") was also studied. A set of the sensor array response data from continuous 6-day human breath tests was collected. PCA analysis of the data is performed with the sensor response data from each day (Figure 7). It is evident that the data for healthy and the LC VOC-spiked breath samples are well separated with little (in the first 5 days) or small (in the last day) overlap among all 6 days, demonstrating high stability.

The sensor array stability can be further assessed by examining the average and standard deviations of the sensor responses toward the human breath samples (Table S3). The average sensor responses of each sensor remain almost the same over the 6-day testing period. The responses collected from repeated tests exhibit a small standard deviation in the  $10^{-4}$  level. The relative standard deviation (RSD) is low as 0.627% for sensor responses to human breath samples and 0.542% for human breaths spiked with lung cancer-specific VOCs. These findings demonstrate the long-term stability performance for our sensor arrays.

# CONCLUSIONS

In summary, the results from both theoretical and experimental evaluations of the sensor array system in the responses to selected panels of VOCs in human breaths have demonstrated the potential applicability of the system in the development of portable and wireless sensors for breath screening of lung cancer in two significant ways. First, the chemiresistive responses of the sensor array to selected panels of breath VOCs with healthy and lung cancer compositions are tunable in terms of the nanostructural parameters, which is supported

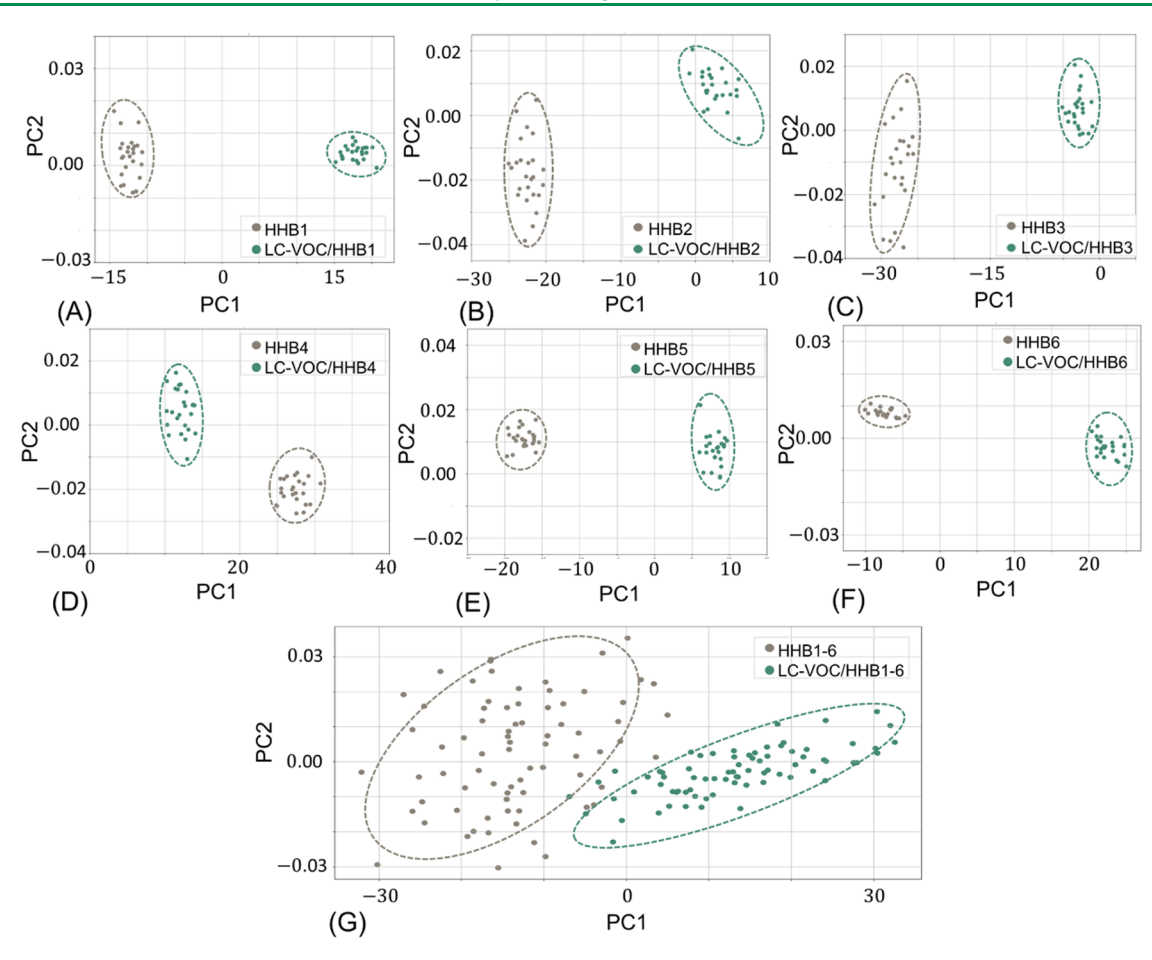


Figure 6. PCA plots of sensor responses to human breath samples with and without lung cancer-specific VOCs (toluene, 2-butanone, and 2,3,4-trimethyl-pentane, each at 9 ppm). (A–F) different individuals. (G) PCA plots of the sensor array responses to human breath samples with and without lung cancer-specific VOCs.

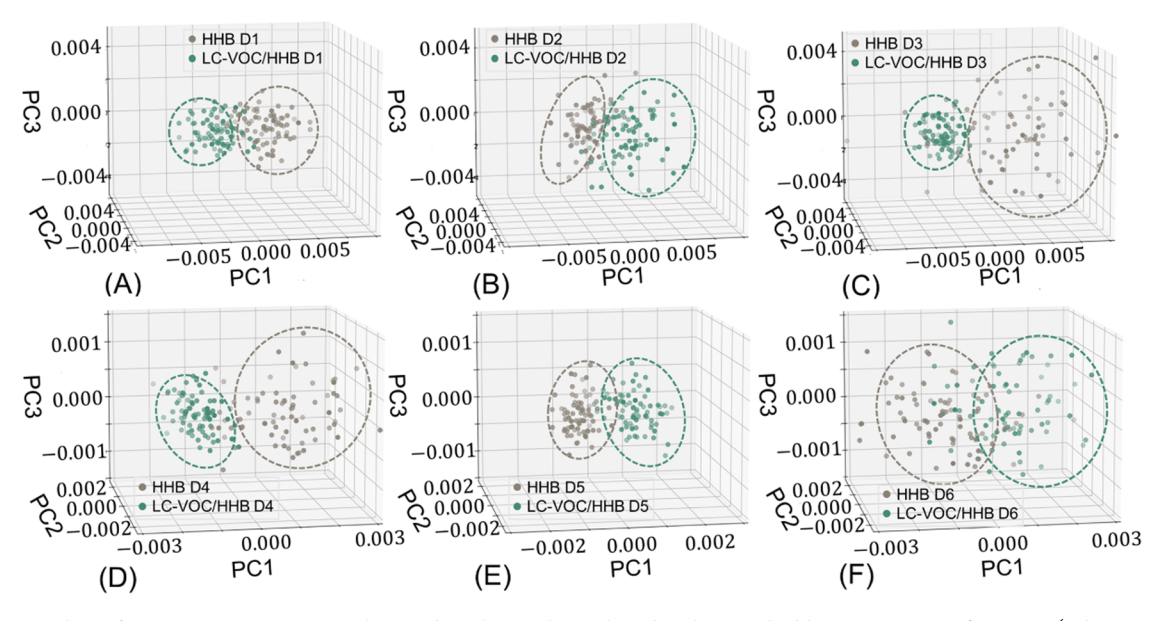


Figure 7. PCA plots of sensor array responses to human breath samples with and without spiked lung cancer-specific VOCs (toluene, 2-butanone, and 2,3,4-trimethyl-pentane, each at 9 ppm) over a period of consecutive 6 days (A–F: day 1 to day 6).

by the theoretical simulation results showing the ability in recognition of lung cancer VOCs. Second, the sensor system has demonstrated the viability of discrimination between the human breaths with lung cancer-specific VOCs and controls,

which is supported by the results from testing healthy human breaths spiked quantitatively with the lung cancer-relevant VOCs. Moreover, the sensor system has shown high sensitivity and selectivity in the detection, featuring a limit of detection as low as 6 ppb. Moreover, the sensor system has also demonstrated a stable performance in recognizing breaths from simulated lung cancer breaths and healthy breaths under ambient conditions. These results, in combination with the device portability and wireless data requisition and processing capabilities in terms of cost effectiveness, ease of use, and rapid analysis time, also provide useful information for clinical testing toward the development of a point-of-care sensor for early-stage lung cancer detection, which are part of our ongoing investigations.

#### ASSOCIATED CONTENT

# **Solution** Supporting Information

The Supporting Information is available free of charge at https://pubs.acs.org/doi/10.1021/acssensors.2c02839.

Table of the simulation parameters of the sensor arrays used in this work; table of the lung cancer-related VOCs panel; and table of the statistics of the sensor responses to breath samples (PDF)

# AUTHOR INFORMATION

#### **Corresponding Authors**

Chuan-Jian Zhong — Department of Chemistry, State University of New York at Binghamton, Binghamton, New York 13902, United States; orcid.org/0000-0003-0746-250X; Email: cjzhong@binghamton.edu

Susan Lu — Systems Science and Industrial Engineering, State University of New York at Binghamton, Binghamton, New York 13902, United States; Email: slu@binghamton.edu

#### **Authors**

Guojun Shang — Department of Chemistry, State University of New York at Binghamton, Binghamton, New York 13902, United States

Dong Dinh – Systems Science and Industrial Engineering, State University of New York at Binghamton, Binghamton, New York 13902, United States

Tara Mercer – Department of Chemistry, State University of New York at Binghamton, Binghamton, New York 13902, United States

Shan Yan — Department of Chemistry, State University of New York at Binghamton, Binghamton, New York 13902, United States

Shan Wang – Department of Chemistry, State University of New York at Binghamton, Binghamton, New York 13902, United States

Behnaz Malaei – Systems Science and Industrial Engineering, State University of New York at Binghamton, Binghamton, New York 13902, United States

Jin Luo – Department of Chemistry and Systems Science and Industrial Engineering, State University of New York at Binghamton, Binghamton, New York 13902, United States; orcid.org/0000-0002-4363-8886

Complete contact information is available at: https://pubs.acs.org/10.1021/acssensors.2c02839

#### **Author Contributions**

The manuscript was written through contributions of all authors. All authors have given approval to the final version of the manuscript.

#### Notes

The authors declare no competing financial interest.

#### ACKNOWLEDGMENTS

This research was funded by the National Science Foundation (IIP 1640669, and CHE 2102482), in part by Binghamton University Harpur College Faculty Research Seed Grant and Watson—United Health Services (UHS) Collaboration Seed Grant, and IEEC.

#### REFERENCES

- (1) Deo, S. V. S.; Sharma, J.; Kumar, S. GLOBOCAN 2020 Report on Global Cancer Burden: Challenges and Opportunities for Surgical Oncologists. *Ann. Surg. Oncol.* 2022, 29, 6497–6500.
- (2) Ferlay, J.; Colombet, M.; Soerjomataram, I.; Parkin, D. M.; Piñeros, M.; Znaor, A.; Bray, F. Cancer Statistics for the Year 2020: An Overview. *Int. J. Cancer* 2021, *149*, 778–789.
- (3) Jemal, A.; Siegel, R. L.; Miller, K. D. Cancer Statistics. *CA-Cancer J. Clin.* **2017**, *67*, 7–30.
- (4) The National Lung Screening Trial Research Team. Reduced Lung-Cancer Mortality with Low-Dose Computed Tomographic Screening. N. Engl. J. Med. 2011, 365, 395–409.
- (5) Davies, T.; Hayward, N. Volatile Products from Acetylcholine as Markers in the Rapid Urine Test using Head-space Gas-liquid Chromatography. *J. Chromatogr. B: Biomed. Sci. Appl.* **1984**, 307, 11–21.
- (6) Peng, G.; Tisch, U.; Adams, O.; Hakim, M.; Shehada, N.; Broza, Y. Y.; Billan, S.; Abdah-Bortnyak, R.; Kuten, A.; Haick, H. Diagnosing Lung Cancer in Exhaled Breath using Gold Nanoparticles. *Nat. Nanotechnol.* **2009**, *4*, 669–673.
- (7) Peng, G.; Hakim, M.; Broza, Y. Y.; Billan, S.; Abdah-Bortnyak, R.; Kuten, A.; Tisch, U.; Haick, H. Detection of Lung, Breast, Colorectal, and Prostate Cancers from Exhaled Breath using a Single Array of Nanosensors. *Br. J. Cancer* **2010**, *103*, 542–551.
- (8) Barash, O.; Peled, N.; Tisch, U.; Bunn, P. A.; Hirsch, F. R.; Haick, H. Classification of Lung Cancer Histology by Gold Nanoparticle Sensors. *Nanotechnol. Biol. Med.* **2012**, *8*, 580–589.
- (9) Yu, H.; Xu, L.; Cao, M.; Chen, X.; Wang, P.; Jiao, J.; Wang, Y. In Detection Volatile Organic Compounds in Breath as Markers of Lung Cancer using a Novel Electronic Nose, IEEE Sensors, Proceedings of the Second IEEE International Conference on Sensors, Toronto, Canada, October 22-24, 200320032; IEEE Sensors Council Academic Publishers: Piscataway: The United States of America, 2003; pp 1333–1337.
- (10) Peng, G.; Trock, E.; Haick, H. Detecting Simulated Patterns of Lung Cancer Biomarkers by Random Network of Single-walled Carbon Nanotubes Coated with Nonpolymeric Organic Materials. *Nano Lett.* **2008**, *8*, 3631–3635.
- (11) Wang, L.; Shi, X.; Karjuki, N. N.; Schadt, M.; Wang, G. R.; Rendeng, Q.; Choi, J.; Luo, J.; Lu, S.; Zhong, C. J. Array of Molecularly-mediated Thin Film Assemblies of Nanoparticles: Correlation of Vapor Sensing with Interparticle Spatial Properties. *J. Am. Chem. Soc.* **2007**, *129*, 2161–2170.
- (12) Zhao, W.; Al-Nasser, L. F.; Shan, S.; Li, J.; Skeete, Z.; Kang, N.; Luo, J.; Lu, S.; Zhong, C. J.; Grausgruber, C. J.; Harris, R. Detection of Mixed Volatile Organic Compounds and Lung Cancer Breaths Using Chemiresistor Arrays with Crosslinked Nanoparticle Thin Films. Sens. Actuators, B 2016, 232, 292–299.
- (13) Brust, M.; Walker, M.; Bethell, D.; Schiffrin, D. J.; Whyman, R. Synthesis of Thiol-derivatised Gold Nanoparticles in a Two-phase Liquid-liquid System. *J. Chem. Soc., Chem. Commun.* **1994**, *0*, 801–802.
- (14) Hostetler, M. J.; Wingate, J. E.; Zhong, C. J.; Harris, J. E.; Vachet, R. W.; Clark, M. R.; Londono, J. D.; Green, S. J.; Stokes, J. J.; Wignall, G. D.; Glish, G. L.; Porter, M. D.; Evans, N. D.; Murray, R. W. Alkanethiolate Gold Cluster Molecules with Core Diameters from 1.5 to 5.2 nm: Core and Monolayer Properties as a Function of Core Size. *Langmuir* 1998, *14*, 17–30.
- (15) Maye, M. M.; Zheng, W. X.; Leibowitz, F. L.; Ly, N. K.; Zhong, C. J. Heating-induced Evolution of Thiolate-encapsulated Gold

**ACS Sensors** Article pubs.acs.org/acssensors

Nanoparticles: A Strategy for Size and Shape Manipulations. Langmuir 2000, 16, 490-497.

- (16) Schadt, M. J.; Cheung, W.; Luo, J.; Zhong, C. J. Molecularlytuned Size Selectivity in Thermal Processing of Gold Nanoparticles. Chem. Mater. 2006, 18, 5147-5149.
- (17) Wang, L.; Luo, J.; Schadt, M.; Zhong, C. J. Thin Film Assemblies of Molecularly-linked Metal Nanoparticles and Multifunctional Properties. Langmuir 2010, 26, 618-632.
- (18) Wang, L.; Kariuki, N. N.; Schadt, M.; Mott, D.; Luo, J.; Zhong, C. J.; Shi, X.; Zhang, C.; Hao, W.; Lu, S.; Kim, N.; Wang, J. Q. Sensing Arrays Constructed from Nanoparticle Thin Films and Interdigitated Microelectrodes. Sensors 2006, 6, 667-679.
- (19) Leibowitz, F. L.; Zheng, W. X.; Maye, M. M.; Zhong, C. J. Structures and Properties of Nanoparticle Thin Films Formed via a One-step Exchange-crosslinking-precipitation Route. Anal. Chem. 1999, 71, 5076-5083.
- (20) Wang, G. R.; Wang, L.; Rendeng, Q.; Wang, J.; Luo, J.; Zhong, C. J. Correlation Between Nanostructural Parameters and Conductivity Properties for Thin Film Assemblies of Gold Nanoparticles. J. Mater. Chem. 2007, 17, 457-462.
- (21) Wohltjen, H.; Snow, A. W. Colloidal Metal-insulator-metal Ensemble Chemiresistors Sensor. Anal. Chem. 1998, 70, 2856-2859.
- (22) Steinecker, W. H.; Rome, M. P.; Zellers, E. T. Model of Vaporinduced Resistivity Changes in Gold-thiolate Monolayer-protected Nanoparticle Sensor Film. Anal. Chem. 2007, 79, 4977-4986.
- (23) Yin, J.; Hu, P.; Luo, J.; Wang, L.; Cohen, M. F.; Zhong, C. J. Molecularly-mediated Thin Film Assembly of Nanoparticles on Flexible Devices: Electrical Conductivity vs. Device Strains in Different Gas/Vapor Environment. ACS Nano 2011, 5, 6516-6526.
- (24) Shan, S.; Zhao, W.; Luo, J.; Yin, J.; Switzer, J. C.; Joseph, P.; Lu, S.; Poliks, M.; Zhong, C. J. Flexibility Characteristics of Polyethylene Terephthalate Chemiresistor Coated with a Nanoparticle Thin Film Assembly. J. Mater. Chem. C 2014, 2, 1893-1903.
- (25) Olichuer, N.; Meyer, A.; Yesilmen, M.; Vossmeyer, T. Gold Nanoparticles Superlattices: Correlating Chemiresistive Responses with Analyte Sorption and Swelling. J. Mater. Chem. C 2016, 4, 8214-
- (26) Belmares, M.; Blanco, M.; Goddard, W. A.; Ross, R. B.; Caldwell, G.; Chou, S. H.; Pham, J.; Olofson, P. M.; Thomas, C. Hildebrand and Hanson Solubility Parameters from Molecular Dynamics with Applications to Electronic Nose Polymer Sensors. J. Comput. Chem. 2004, 25, 1814-1826.
- (27) Belmares, M. P. Molecular Origins of the Thermophysical Properties of Polymers and Modeling of Polymer Permeation by Large Molecules. Ph.D. Dissertation, California Institute of Technology, Pasadena, CA, 1998. https://resolver.caltech.edu/CaltechET-D:etd-12172004-155023 (accessed March 02, 2020).
- (28) García-Berríos, E.; Gao, T.; Theriot, J. C.; Woodka, M. D.; Brunschwig, B. S.; Lewis, N. S. Response and Discrimination Performance of Arrays of Organothiol-capped Au Nanoparticle Chemiresistive Vapor Sensors. J. Phys. Chem. C 2011, 115, 6208-6217.
- (29) Gao, T.; Woodka, M. D.; Brunschwig, B. S.; Lewis, N. S. Chemiresistors for Array-Based Vapor Sensing Using Composites of Carbon Black with Low Volatility Organic Molecules. Chem. Mater. 2006, 18, 5193-5202.
- (30) Lonergan, M. C.; Severin, E. J.; Doleman, B. J.; Beaber, S. A.; Grubbs, R. H.; Lewis, N. S. Array-Based Vapor Sensing Using Chemically Sensitive, Carbon Black-Polymer Resistors. Chem. Mater. **1996**, 8, 2298-2312.
- (31) Yan, S.; Liu, X.; Skeete, Z.; He, N.; Xie, Z. H.; Zhao, W.; Lombardi, J. P.; Liu, K.; Kang, N.; Luo, J.; Hsiao, B. S.; Poliks, M.; Gitsov, I.; Zhong, C. J. Decoration of Nanofibrous Paper Chemiresistors with Dendronized Nanoparticles towards Structurally-tunable Negative-going Response Characteristics to Human Breathing and Sweating. Adv. Mater. Interfaces 2017, 4, 1700380-1700391.
- (32) Kang, N.; Lin, F.; Zhao, W.; Lombardi, J. P.; Almihdhar, M.; Liu, K.; Yan, S.; Kim, J.; Luo, J.; Hsiao, B. S.; Poliks, M.; Zhong, C. J.

Nanoparticle-nanofibrous Membranes as Scaffolds for Flexible Sweat Sensors. ACS Sens. 2016, 1, 1060-1069.

(33) Yan, S.; Shan, S.; Wen, J.; Li, J.; Kang, N.; Wu, Z.; Lombardi, J.; Cheng, H. W.; Wang, J.; Luo, J.; He, N.; Mott, D.; Wang, L.; Ge, Q.; Hsiao, B. S.; Poliks, M.; Zhong, C. J. Surface-mediated Interconnections of Nanoparticles in Cellulosic Fibrous Materials Towards 3D Sensors. Adv. Mater. 2020, 32, 2002171-2002180.

# **□** Recommended by ACS

# **Artificial Olfactory Signal Modulation for Detection in Changing Environments**

Mohamed F. Hassan, Michael S. Freund, et al.

FEBRUARY 13, 2023

ACS SENSORS

READ 2

# Machine Learning-Assisted Sensor Based on CsPbBr<sub>3</sub>@ZnO Nanocrystals for Identifying Methanol in Mixed **Environments**

Wufan Xuan, Sheng Huang, et al.

MARCH 10, 2023

ACS SENSORS

READ

## Fully Flexible MXene-based Gas Sensor on Paper for Highly **Sensitive Room-Temperature Nitrogen Dioxide Detection**

Wenjing Quan, Zhi Yang, et al.

JANUARY 12, 2023

ACS SENSORS

RFAD 17

## **Liquid Biopsy-Based Volatile Organic Compounds from Blood and Urine and Their Combined Data Sets for Highly Accurate Detection of Cancer**

Reef Einoch Amor, Hossam Haick, et al.

MARCH 16, 2023

**ACS SENSORS** 

RFAD 🗹

Get More Suggestions >